Electron states and electron Raman scattering in semiconductor double cylindrical quantum well wire

M Munguía-Rodríguez[1], Ri Betancourt-Riera[2], Re Betancourt-Riera[2,†], R Riera[1], and J M Nieto Jalil[3]

[1] *Departamento de Investigación en Física, Universidad de Sonora, Apartado Postal* 5-88, 83190, *Hermosillo, Sonora, México*
[2] *Instituto Tecnológico de Hermosillo. Avenida Tecnológico S/N, Col. Sahuaro*, 83170, *Hermosillo, Sonora, México*
[3] *Tecnológico de Monterrey-Campus Sonora Norte. Bulevar Enrique Mazón López No.* 965, 83000, *Hermosillo, Sonora, México*

(Received 2 June 2016; revised manuscript received 20 July 2016; published online 30 September 2016)

The differential cross section for an electron Raman scattering process in a semiconductor GaAs/AlGaAs double quantum well wire is calculated, and expressions for the electronic states are presented. The system is modeled by considering $T = 0$ K and also with a single parabolic conduction band, which is split into a subband system due to the confinement. The gain and differential cross-section for an electron Raman scattering process are obtained. In addition, the emission spectra for several scattering configurations are discussed, and interpretations of the singularities found in the spectra are given. The electron Raman scattering studied here can be used to provide direct information about the efficiency of the lasers.

Keywords: electron states, Raman scattering, selection rules, quantum well wires

PACS: 73.21.Hb, 78.67.Lt **DOI:** 10.1088/1674-1056/25/11/117302

1. Introduction

The Raman scattering is a useful technique to study the electronic structure of nanostructures. The analysis of the differential cross section of a Raman scattering process allows us to determine the subband structure of the nanostructured systems by a direct inspection of singularity positions in the spectra, considering the selection rules of transitions of the electron (or other quasiparticles) in the interaction with different polarizations of the incident and emitted light.[1–3] In general, the differential cross section of a Raman scattering process shows singularities related to the interband and intraband transitions, in our case, only the intraband transitions are considered.

The electron Raman scattering has been studied from a theoretical point of view in various systems. These studies considered the interband and intraband transitions with and without the participation of confinement phonons, also in the presence and absence of external electric and magnetic fields;[4–14] the bulk semiconductor, considering the presence of electric and magnetic fields, was also studied.[15–17] Surface enhanced Raman scattering is one of the most powerful probing methods, which is non-destructive, real-time, and good at highly sensitive characterization.[18,19] Raman scattering studies of phonon modes are of fundamental importance for understanding the structural and optical properties, the surface states can lead to novel magnetic properties.[7,20,21] In the previous studies, the surface optical phonon mode, which is sensitive to the shell thickness, has been found in core/shell quantum dots and core–shell structured nanoparticles. Recently, it has been proposed to be realized in commonly used semiconductors, which suggests a promising approach to the development of semiconductor electronic devices.[21]

The development of several experimental techniques has allowed the nanometer-scale confinements of the band electrons in semiconductor materials to provide some varieties of quantum phenomena, such as low-dimensional electron states and modified dynamics of carriers in the systems. Thus, the study of electron Raman scattering remains as an interesting and fundamental issue.[22] Recently, the experimental research on the Raman scattering in the GaN semiconductor quantum well wire of cylindrical ring geometry has been reported.[23–27] In particular, semiconductor double quantum well wire and multiple quantum wells have awakened great interest because these systems allow the development of light sources such as light emitting diodes, and laser diodes in a wide range of the electromagnetic spectrum from ultraviolet to terahertz. These systems were used because they offer the possibility to create an artificial three-level system[28,29] given the possibility of controlling the parameters of the quantum well wire such as width and height of the potential barrier. These devices are manufactured using different methods, and several types of materials, such as InGaAs/AlInAs and GaAs/AlGaAs.

In this work, we present a model of electron Raman scattering in double quantum well wire, where an electron is in the conduction band. The intraband Raman scattering processes can be qualitatively described in the following way: first, an electron in the conduction band absorbs a photon of incident radiation of energy, $\hbar\omega_{\rm l}$, resulting in an intersubband transition; then the electron emits a photon of secondary radiation of energy, $\hbar\omega_{\rm s}$, due to a new intersubband transition.

†Corresponding author. E-mail: rbriera@gmail.com

© 2016 Chinese Physical Society and IOP Publishing Ltd

2. Model and electronic states

We must determine the stationary states of an electron in a double quantum well wire system of cylindrical geometry, where r_a, r_b, and r_c are the radii and length L. The confinement potential (V_c) and the effective mass (μ) are given by

$$V_c, \quad \mu = \begin{cases} 0, & \mu_1, & 0 \le r \le r_a, \\ V_0, & \mu_2, & r_a < r < r_b, \\ 0, & \mu_1, & r_b \le r \le r_c, \\ V_0, & \mu_2, & r_c < r < \infty. \end{cases}$$

The envelope function approximation leads to the solution of Schrödinger equation

$$\Psi(\boldsymbol{r}) = \frac{\exp[\mathrm{i}(m\theta + k_z z)]}{\sqrt{2\pi L}} u_0(\boldsymbol{r})\, \varphi_{n,m}(r), \tag{1}$$

where

$$\varphi_{n,m}(r) = \begin{cases} A_1 \mathrm{J}_m(x), & 0 \le r < r_a, \\ A_2 \mathrm{I}_m(y) + B_2 \mathrm{K}_m(y), & r_a \le r < r_b, \\ A_3 \mathrm{J}_m(x) + B_3 \mathrm{N}_m(x), & r_b \le r < r_c, \\ B_4 \mathrm{K}_m(y), & r_c \le r < \infty, \end{cases} \tag{2}$$

where $u_0(\boldsymbol{r})$ is the electron Bloch function in the band; J_m and N_m are the Bessel functions of the first and the second kind of order m; I_m and K_m are the modified Bessel functions of the first and the second kind of order m. Here, we use the definitions of Bessel functions according to Abramowitz.[30] The electron energy is given by

$$E_{n,m}(k_z) = E_r(n,m) + \frac{\hbar^2}{2\mu_{1(2)}} k_z^2,$$

where

$$x(r) = \sqrt{\frac{2\mu_2 r^2}{\hbar^2} E_r}, \quad y(r) = \sqrt{\frac{2\mu_1 r^2}{\hbar^2}(V_0 - E_r)},$$
$$\beta = \sqrt{\frac{\mu_1}{\mu_2}\frac{V_0 - E_r}{E_r}},$$

where E_r is the energy due to the spatial confinement. By considering the continuity of the function Ψ and the current density $(1/\mu)(\partial\Psi/\partial r)$ at the interface, we can calculate the constants A and B present in Eq. (2); also can determine energy levels E_r, then

$$A_2 = \frac{A_{21}}{C_2} A_1, \quad B_2 = -\frac{B_{21}}{C_2} A_1,$$
$$A_3 = \frac{A_{21}A_{31} - B_{21}A_{32}}{C_2 C_3} A_1, \quad B_3 = -\frac{A_{21}B_{31} - B_{21}B_{32}}{C_2 C_3} A_1,$$
$$B_4 = \frac{(A_{21}A_{31} - B_{21}A_{32})\mathrm{J}_m(x_c) - (A_{21}B_{31} - B_{21}B_{32})\mathrm{N}_m(x_c)}{C_2 \mathrm{K}_m(y_c) C_3} A_1,$$

with

$$\begin{aligned} A_{21} &= \mathrm{J}_m(x_a)\mathrm{K}'_m(y_a) - \beta^{-1}\mathrm{J}'_m(x_a)\mathrm{K}_m(y_a), \\ B_{21} &= \mathrm{J}_m(x_a)\mathrm{I}'_m(y_a) - \beta^{-1}\mathrm{J}'_m(x_a)\mathrm{I}_m(y_a), \\ C_2 &= \mathrm{I}_m(y_a)\mathrm{K}'_m(y_a) - \mathrm{I}'_m(y_a)\mathrm{K}_m(y_a), \\ A_{31} &= \mathrm{I}_m(y_b)\mathrm{N}'_m(x_b) - \beta\mathrm{I}'_m(y_b)\mathrm{N}_m(x_b), \\ A_{32} &= \mathrm{K}_m(y_b)\mathrm{N}'_m(x_b) - \beta\mathrm{K}'_m(y_b)\mathrm{N}_m(x_b), \\ B_{31} &= \mathrm{I}_m(y_b)\mathrm{J}'_m(x_b) - \beta\mathrm{I}'_m(y_b)\mathrm{J}_m(x_b), \\ B_{32} &= \mathrm{K}_m(y_b)\mathrm{J}'_m(x_b) - \beta\mathrm{K}'_m(y_b)\mathrm{J}_m(x_b), \\ C_3 &= \mathrm{J}_m(x_b)\mathrm{N}'_m(x_b) - \mathrm{J}'_m(x_b)\mathrm{N}_m(x_b), \end{aligned}$$

being $x_k = x(r_k)$ and $y_k = y(r_k)$, A_1 can be obtained using the normalization condition, therefore,

$$A_1 = [I_1 + I_2 + I_3 + I_4]^{-1/2},$$

where

$$I_1 = \int_0^{r_a} \mathrm{J}_m^2(x)\, r\mathrm{d}r, \quad I_2 = \frac{1}{C_2^2}\int_{r_a}^{r_b} [A_{21}I_m(y) - B_{21}\mathrm{K}_m(y)]^2\, r\mathrm{d}r,$$
$$I_3 = \frac{1}{C_2^2 C_3^2}\int_{r_b}^{r_c} \big[(A_{21}A_{31} - B_{21}A_{32})\mathrm{J}_m(x) - (A_{21}B_{31} - B_{21}B_{32})\mathrm{N}_m(x)\big]^2 r\mathrm{d}r,$$
$$I_4 = \left[\frac{(A_{21}A_{31} - B_{21}A_{32})\mathrm{J}_m(x_c) - (A_{21}B_{31} - B_{21}B_{32})\mathrm{N}_m(x_c)}{C_2 \mathrm{K}_m(y_c) C_3}\right]^2 \times \int_{r_c}^{\infty} \mathrm{K}_m^2(y)\, r\mathrm{d}r.$$

In addition, E_r is determined from the following transcendental equation:

$$(A_{21}A_{31} - B_{21}A_{32})A_{41} = (A_{21}B_{31} - B_{21}B_{32})A_{42}, \tag{3}$$

where

$$\begin{aligned} A_{41} &= \mathrm{J}_m(x_c)\mathrm{K}'_m(y_c) - \beta^{-1}\mathrm{J}'_m(x_c)\mathrm{K}_m(y_c), \\ A_{42} &= \mathrm{N}_m(x_c)\mathrm{K}'_m(y_c) - \beta^{-1}\mathrm{N}'_m(x_c)\mathrm{K}_m(y_c). \end{aligned}$$

As it can be observed, for each value of m, n energy values are obtained. The states are then described by the following quantum numbers: $m = 0, 1, 2, \ldots$; $n = 1, 2, 3, \ldots$; and k_z (see Ref. [27]). We can say that the system is the combination of a quantum well wire of cylindrical disk geometry in the region where $r \le r_a$, which we call "the wire", and a quantum well wire with a cylindrical ring geometry in the region where $r_b \le r \le r_c$, which we call "the shell"; while the barrier is the region where $r_a < r < r_b$.

3. Raman cross-section

The Raman differential cross-section in a volume per unit solid angle for incoming light of frequency ω_l and scattered

light of frequency ω_s is given in Ref. [12], and it can be written as

$$\frac{d^2\sigma}{d\omega_s d\Omega} = \frac{V^2\omega_s^2\eta(\omega_s)}{8\pi^3c^4\eta(\omega_l)}W(\omega_l,e_l,\omega_s,e_s), \quad (4)$$

where $\eta(\omega_\rho)$ is the refraction index as a function of the radiation with frequency ω_ρ and polarization unit vector is e_ρ. The subindex $\rho = l(s)$ indicates the incident (secondary) radiation; c is the light velocity in a vacuum, V is the volume, and $W(\omega_l,e_l,\omega_s,e_s)$ is the transition rate for the absorption and emission radiation calculated according to Fermi's golden rule. In this case, two possibilities must be considered: (i) the electron absorbs the incident photon and it later emits the secondary radiation photon; or (ii) the electron emits the secondary radiation photon and later absorbs the incident photon.[28] Therefore,

$$W(\omega_l,e_l,\omega_s,e_s) = \frac{2\pi}{\hbar}\sum_f |M_f|^2\delta(E_f - E_i),$$

where

$$M_f = \sum_a \frac{\langle f|\hat{H}_s|a\rangle\langle a|\hat{H}_l|i\rangle}{E_i - E_a + i\Gamma_a} + \sum_b \frac{\langle f|\hat{H}_l|b\rangle\langle b|\hat{H}_s|i\rangle}{E_i - E_b + i\Gamma_b}; \quad (5)$$

in which $|i\rangle$ and $|f\rangle$ are the initial and final states with energies E_i and E_f, respectively; $|a\rangle$ and $|b\rangle$ are the intermediate states with energies E_a and E_b, respectively; and finally Γ_a and Γ_b are their respective lifetimes.[1]

The Hamiltonian operator for the radiation field $\hat{H}_\rho$, with frequency ω_ρ and polarization unit vector e_ρ, is commonly used in electron Raman scattering and resonant Raman scattering in nanostructures in the dipole approximation. This approximation is valid as long as the radiation wavelength is much larger than the radius of the wire. The effect of reduced dimensionality on the free carrier absorption and the selection rules for intersubband transition have been discussed in Ref. [28], where it is shown that the electron Raman scattering can only take place in the confinement direction, then

$$\hat{H}_\rho = \sqrt{\frac{2\pi\hbar e^2}{V\omega_\rho}}\frac{(\hat{e}_\rho\cdot\hat{p})}{\mu}, \quad \hat{p} = -i\hbar(\nabla_+ e_- + \nabla_- e_+), \quad (6)$$

with μ the electron effective mass, and

$$\nabla_\pm = \frac{\exp(\pm i\theta)}{\sqrt{2}}\left[\frac{\partial}{\partial r} \pm \frac{i}{r}\frac{\partial}{\partial\theta}\right], \quad e_\pm = \frac{e_x \pm ie_y}{\sqrt{2}}.$$

Now, we must calculate the matrix elements appearing in Eq. (5). We use the condition $k = 0$ for the radiation field;[28] thus, by considering Eqs. (1) and (6), the following matrix elements can be obtained:

$$\left\langle \Psi_{m',n',k_z'}\left|\hat{H}_\rho\right|\Psi_{m'',n'',k_z''}\right\rangle_\pm = -i\hbar\frac{|e|}{\mu_0 r_0}\sqrt{\frac{2\pi\hbar}{V\omega_\rho}}(e_\rho\cdot e_\pm)T_\pm(m',m'')\delta_{m'\pm1,m''}\delta_{k_z',k_z''}, \quad (7)$$

where $\Psi_{m',n',k_z'}$ and $\Psi_{m'',n'',k_z''}$ are the final and initial states of the transition, respectively, and

$$T_\pm(m',m'') = I_{m'm''} \mp m'' II_{m'm''}, \quad r_0 = \frac{r_a(r_c - r_b)}{r_a - r_b + r_c},$$

and μ_0 is the electron free mass.

The explicit forms of $I_{m'm''}$ and $II_{m'm''}$ are very complicated and their expressions can be calculated following the method reported in Ref. [31]. As it can be observed, the emission or absorption of one photon can only take place between consecutive states of the quantum number m, according to the selection rules $m'' = m' \pm 1$, although there is no restriction for the quantum number n (see Eq. (7)).

In the initial state, we have an electron in a conduction subband and an incident radiation photon; and for the final state, we have an electron in the other conduction subband and a secondary radiation photon

$$E_i = \hbar\omega_l + E_{m'',n''}(k_z), \quad E_f = \hbar\omega_s + E_{m,n}(k_z). \quad (8)$$

For the intermediate states

$$E_a = E_{m',n'}(k_z), \quad E_b = \hbar\omega_l + \hbar\omega_s + E_{m',n'}(k_z). \quad (9)$$

Using Eqs. (7)–(9), we can obtain four different contributions to the differential cross section (see Ref. [27]), depending on the polarizations of the incident and emitted radiation, and finally we can rewrite Eq. (4) as

$$\left[\frac{d^2\sigma}{d\omega_s d\omega}\right] = \left[\frac{d^2\sigma}{d\omega_s d\omega}\right]_{++} + \left[\frac{d^2\sigma}{d\omega_s d\omega}\right]_{+-} + \left[\frac{d^2\sigma}{d\omega_s d\omega}\right]_{-+} + \left[\frac{d^2\sigma}{d\omega_s d\omega}\right]_{--},$$

where

$$\left[\frac{d^2\sigma}{d\omega_s d\omega}\right]_{\pm\pm} = \sigma_0\left(\sigma_s^\pm\cdot\sigma_l^\pm\right)^2\sum_{m,n,n''}\frac{|M_{\pm\pm}|^2}{[\hbar\omega_l - \hbar\omega_s + E_r(m\pm2,n'') - E_r(m,n)]^2 + \Gamma_f^2}, \quad (10)$$

$$\left[\frac{d^2\sigma}{d\omega_s d\omega}\right]_{\mp\pm} = \sigma_0\left(\sigma_s^\pm\cdot\sigma_l^\mp\right)^2\sum_{m,n,n''}\frac{|M_{\mp\pm}|^2}{[\hbar\omega_l - \hbar\omega_s + E_r(m,n'') - E_r(m,n)]^2 + \Gamma_f^2}, \quad (11)$$

$$M_{\pm\pm} = \frac{\hbar^2}{2\mu_0 r_0^2}\sum_n{}' T_\pm(m,m\mp1)T_\pm(m\mp1,m\mp2)\left[\frac{1}{\hbar\omega_s + E_r(m,n) - E_r(m\pm1,n') + i\Gamma_a}\right.$$

$$-\frac{1}{\hbar\omega_{\rm l}-E_r(m,n)+E_r(m\pm1,n')-{\rm i}\Gamma_b}\Bigg], \tag{12}$$

$$M_{\mp\pm}=\frac{\hbar^2}{2\mu_0 r_0^2}\sum_n{}'T_{\mp}(m,m\pm1)\,T_{\pm}(m\pm1,m)\left[\frac{1}{\hbar\omega_{\rm s}+E_r(m,n)-E_r(m\pm1,n')+{\rm i}\Gamma_a}-\frac{1}{\hbar\omega_{\rm l}-E_r(m,n)+E_r(m\pm1,n')-{\rm i}\Gamma_b}\right], \tag{13}$$

$$\sigma_\rho^{\pm}=\boldsymbol{e}_\rho\cdot\boldsymbol{e}_{\pm},\qquad \sigma_0=\frac{\eta(\omega_{\rm s})}{\eta(\omega_{\rm l})}\left(\frac{e}{c}\right)^4\frac{\hbar\Gamma_f}{\pi r_0\mu_0^2}\frac{\omega_{\rm s}}{\omega_{\rm l}}.$$

4. Discussion of the obtained results

In this case, we considered a cylindrical semiconductor double quantum wire grown in a $GaAs/Al_{0.35}Ga_{0.65}As$ matrix, and the following physical parameters[29] were used in this calculations: $\mu_1=0.096\mu_0$, $\mu_2=0.0665\mu_0$, and $V_0=0.30$ eV, where μ_0 is the free electron mass. Furthermore, in all cases, it is considered that $\Gamma_a=\Gamma_b=\Gamma_f=1$ meV.

Figure 1 shows the electron state energy, E_r of the double quantum well wire (solid lines), obtained using Eq. (3); where the values of r_a and r_c are fixed and r_b takes values in the range of (r_a,r_c). In Figs. 1(a)–1(c), $r_a=6.0$ nm and $r_c=12.0$ nm, $r_a=6.0$ nm and $r_c=14.0$ nm, $r_a=8.0$ nm and $r_c=14.0$ nm, respectively. The dashed lines correspond to the energies of a simple quantum well wire with radius r_a. In this type of system, we can say that levels belong mainly to the wire or to the shell, but we must take into account that the quantum states actually belong to both, i.e., belong to the system; this is what we refer to as "coupling".[32,33] Initially, in Fig. 1, we have a simple quantum well wire with radius r_c, because $r_b=r_a$. As r_b increases, the double quantum well wire is formed; such that the width of the shell, $d=r_c-r_b$, diminishes and increases the width of the barrier, $b=r_b-r_a$. Finally, when $r_b=r_c$, we obtain a simple quantum well wire with radius r_a. In Fig. 1(a), we can see that the electron state denoted by $m=0$ and $n=1$ is the ground state of the system, and is contained primarily in the wire, as it tends to a simple quantum well wire when the radius r_b increases.[32] Besides, using the same argument we can determine that the electron state denoted by $m=0$ and $n=2$ is contained primarily in the shell, being the electron state of the shell with the lowest energy; but this is only true in the region $r_b>6.6$ nm; so this is the point where the system coupling begins to break. We can say that for $0<r_b<6.6$ nm, the system is in strong coupling. It can be observed that for $r_b\approx8.0$ nm, the electron states corresponding to a shell are "taken out" from the system, due to the increase of the confinement of the electrons in this region. Moreover, we can see that the level denoted by $m=0$ and $n=1$ reaches the energy of a simple quantum well wire when $r_b\approx10.0$ nm.

If we compare Fig. 1(b) with Fig. 1(a), the r_c value is increased, $r_c=14.0$ nm, being the immediate consequence of the increase in the number of electronic states "within" the system. Again, we have only one level of the wire, $m=0$ and $n=1$, which is logical as it remains the same value of $r_a=6.0$ nm, and again this is the lowest energy level. We can see that the electron state labeled as $m=0$ and $n=2$, cuts the level of the shell with the electron state, $m=1$ and

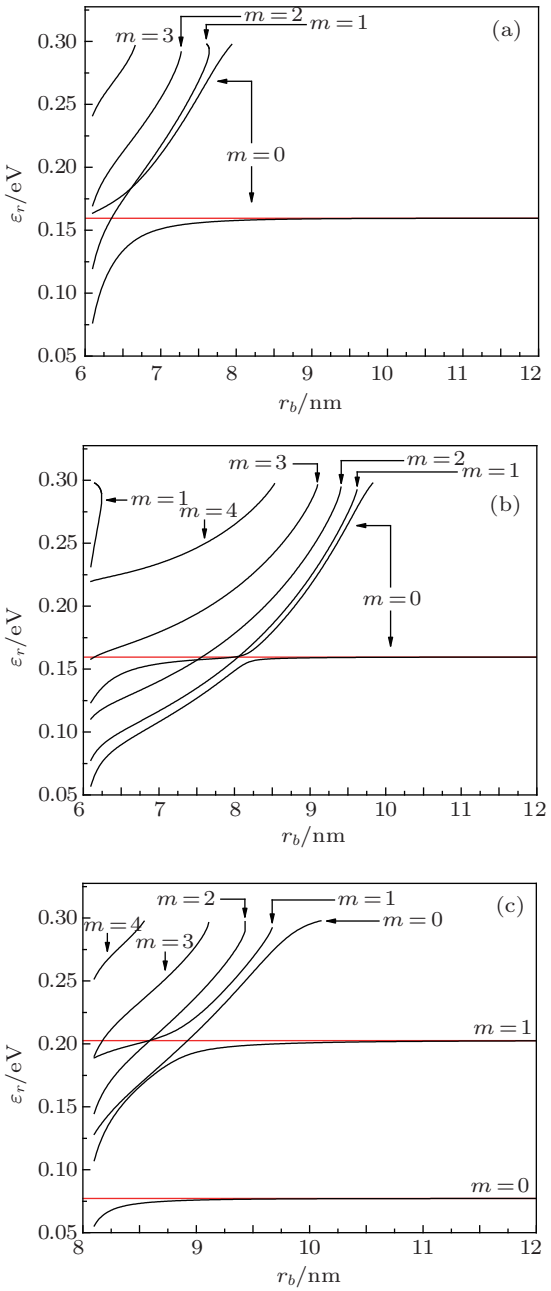


Fig. 1. (color online) Energy of electron states of the double quantum well wire (solid lines), where r_b takes values in the range of (r_a,r_c), while (a) $r_a=6.0$ nm and $r_c=12.0$ nm, (b) $r_a=6.0$ nm and $r_c=14.0$ nm, and (c) $r_a=8.0$ nm and $r_c=14.0$ nm. The dashed lines correspond to the energies of a simple quantum well wire with radius r_a.

$n = 1$, approximately in $r_b = 8.0$ nm, which determines the range where the coupling is strong. In this case, the strong coupling is in the range from $b = 0$ to $b = 2.0$ nm; that is larger than that obtained in Fig. 1(a). This implies that the increase of r_c increases the size of the strong coupling region. Also, it is observed that the electronic states primarily associated with the shell, are organized in subbands determined by the quantum number n, see Fig. 1 of the Ref. [27]. In addition, we see that the electron state, which is denoted by $m = 0$ and $n = 1$, and associated mainly with the wire, reaches the energy of a simple quantum well wire when $r_b \approx 10.0$ nm. Comparing Fig. 1(a) with Fig. 1(b), we can conclude that increasing r_c enlarges the strong coupling region, but practically does not change the point where the electron state denoted by $m = 0$ and $n = 1$ reaches the energy of a simple quantum well wire.

Moreover, in Fig. 1(c), the radii are set as $r_a = 8.0$ nm and $r_c = 14.0$ nm, which means that the radius of the wire is greater than that in Fig. 1(b) while the value of r_c is the same. Comparing these two figures, we can find that the coupling increases because the barrier becomes smaller. Moreover, we can see that with the increase of the radius of the wire, the number of states that "fit" inside also increases, so there are primarily two energy levels associated with the wire. In these electron states mainly related to the wire, it is shown that the higher the energy is, the higher the coupling is, because the "barrier height" that must be overcome by the electrons is lower. When comparing these three figures in Fig. 1, we can see that the states with different values of m can be cut, while if it has the same value of m, it is not possible.

Figure 2 shows the energy of electron states, E_r, for the double quantum well wire (black solid lines), where the barrier varies while the width of the shell is fixed, and the radii of the wire are $r_a = 6.0$ nm and $d = 6.0$ nm, $r_a = 6.0$ nm and $d = 8.0$ nm, and $r_a = 8.0$ nm and $d = 6.0$ nm in Figs. 2(a)–2(c), respectively. The dashed red lines correspond to the quantum state of a quantum well wire of cylindrical ring geometry with width d, while dashed blue lines correspond to the quantum state of a quantum well wire of cylindrical geometry with radius r_a. In Figs. 2(a)–2(c), we can see that all the electron states are corresponding with the band given by $n = 1$, as can be observed in Fig. 2 of Ref . [27]. Furthermore, in the three cases shown in Fig. 2, initially, the barrier does not exist, $b = 0$; this means that initially it has a simple quantum well wire with radius r_c. By comparing Figs. 2(a)–2(c), it can be deduced that the levels associated mainly to the wire do not cut each other, the same situation occurs with levels associated primarily to the shell, if they can cut the levels associated to different system components. In Fig. 2(a), it can be seen that as the barrier increases, the energy levels are adjusted to the energy levels corresponding to a shell (dashed red lines) and to a wire (dashed blue lines). For values of the barrier about 4.0 nm, we cannot find virtually any difference between the levels corresponding to the double quantum well wire and corresponding to the shell and to the wire, for any energy level. If we observe the levels associated with the shell, we can conclude that for higher energy, the decoupling is faster, because the "barrier height" that must be overcome by the electrons is lower. In the case, when electron states are associated primarily to the wire, the value of the barrier required for decoupling is approximately $b = 1.5$ nm, which is lower than that for the shell, so we can say that for the wire the decoupling is faster.

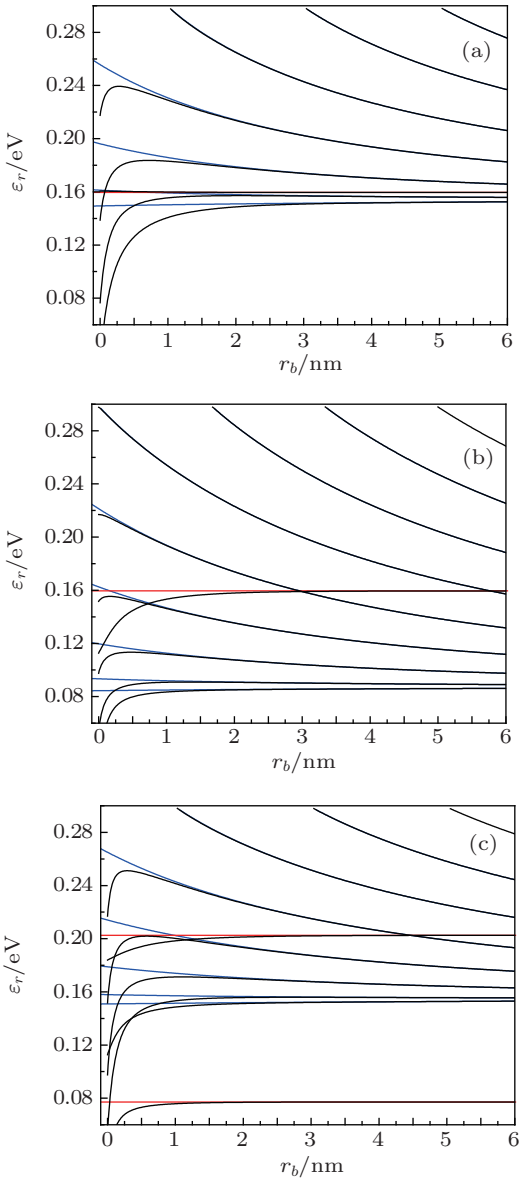


Fig. 2. (color online) Energy of electron states of the double quantum well wire (solid lines) where the barrier $b = r_b - r_a$ varies, while r_a and $d = r_c - r_b$ are maintaining fixed (a) $r_a = 6.0$ nm and $d = 6.0$ nm, (b) $r_a = 6.0$ nm and $d = 8.0$ nm, (c) $r_a = 8.0$ nm and $d = 6.0$ nm. The dotted lines correspond to a quantum well wire of cylindrical ring geometry with width d, while dashed lines correspond to the energies of a simple quantum well wire with radius r_a.

In Fig. 2(b), we increase the width of the shell at $d =$ 8.0 nm, while maintaining the same internal radius, $r_a =$

6.0 nm; this causes an increase in the number of levels mainly associated with the shell that are "within" the system, while it remains the number of associated states primarily to the wire. Comparing Fig. 2(b) with Fig. 2(a), we can see that the energy levels of double quantum wire are made virtually equal to the levels of the shell, from a width of about $b = 2.5$ nm. This means that when the width of the shell is increased, the electron states associated mainly to the shell are decoupled faster; so we can conclude that the coupling is weakened for the states of the shell. However, if we observe the blue dashed lines, it is noted that for the electron states associated primarily to the cable the decoupling requires a higher value of the barrier; in this case approximately $b = 5.0$ nm. Hence, we can conclude that in the case of states of the wire, the increase of d reinforces the coupling. Moreover, in Fig. 2(c) unlike in Fig. 2(a), we increase the value of r_a to 8.0 nm, and the width of the shell, $d = 6.0$ nm remains constant. First, we note that two levels associated with the wire (dashed lines) appear, this is because if the radius is greater, more levels "within" the system can be found. Furthermore, it can be seen that the decoupling of the energy levels associated with the shell occurs to a value similar to the one seen in Fig. 2(a). On the other hand, in the case of the states associated to the wire, we can observe a coupling increase. Therefore, the coupling of the energy levels associated with the shell depends mostly on the width rather than the radius of the wire; while in the case of electron states associated with the wire, the coupling depends on the width and the radius of the shell and the wire, respectively.

Now, we have to analyze the differential cross section of the electron Raman scattering, which can explain the singularities presented in the emission and excitation spectra, respectively. In this case, we must note that equations (12) and (13) have resonant singularities, which are independent of the incident photon, or of the secondary photon when

$$\begin{aligned} &\hbar\omega_\rho\left(m\pm1,n',m,n\right)\rightarrow\hbar\omega_\rho \\ &=\begin{cases} E_r\left(m\pm1,n'\right)-E_r\left(m,n\right), & \rho=\mathrm{s}, \\ E_r\left(m,n\right)+E_r\left(m\pm1,n'\right), & \rho=\mathrm{l}, \end{cases} \end{aligned} \tag{14}$$

where $\rho = \mathrm{s}$ is for the emission spectrum and $\rho = \mathrm{l}$ is for the excitation spectrum. While for Eqs. (10) and (11), we have the non-resonant singularities, which are dependent on the incident photon or the secondary photon for the emission spectrum and for the excitation spectrum, respectively, then

$$\begin{aligned} &SL_\rho\left(m+a,n'',m,n\right)\rightarrow\hbar\omega_\rho \\ &=\begin{cases} \hbar\omega_\mathrm{l}+E_r\left(m\pm a,n''\right)-E_r\left(m,n\right), & \rho=\mathrm{s}, \\ \hbar\omega_\mathrm{s}-E_r\left(m\pm a,n''\right)+E_r\left(m,n\right), & \rho=\mathrm{l}, \end{cases} \end{aligned}$$

where $a = 2$ for $\left(\sigma_\mathrm{s}^+,\sigma_\mathrm{l}^+\right)$ and $\left(\sigma_\mathrm{s}^-,\sigma_\mathrm{l}^-\right)$ polarizations, and $a = 0$ for $\left(\sigma_\mathrm{s}^+,\sigma_\mathrm{l}^-\right)$ and $\left(\sigma_\mathrm{s}^-,\sigma_\mathrm{l}^+\right)$ polarizations. If the energy of the incident radiation is different to the resonance, this difference is named detuning.

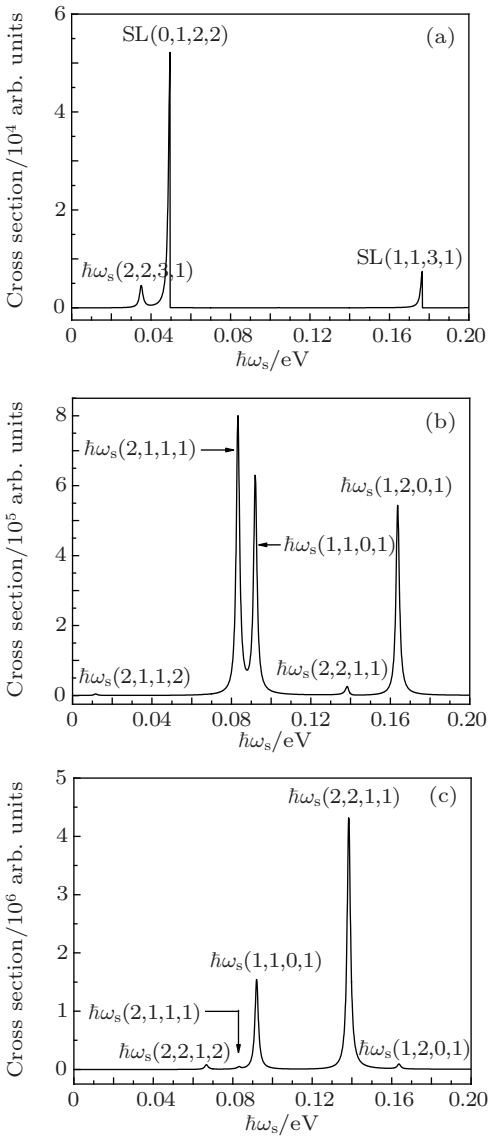


Fig. 3. The emission spectrum for an electron Raman scattering process in double quantum well wire with $r_a = 9.0$ nm, $r_b = 12.0$ nm, and $r_c = 17.0$ nm; for incident photon with energy $\hbar\omega_\mathrm{l} = 0.28$ eV and the polarization: (a) $\left(\sigma_\mathrm{s}^-,\sigma_\mathrm{l}^-\right)$; (b) $\left(\sigma_\mathrm{s}^+,\sigma_\mathrm{l}^+\right)$; (c) $\left(\sigma_\mathrm{s}^-,\sigma_\mathrm{l}^+\right)$.

Figure 3 shows the emission spectrum of a double quantum well wire with $r_a = 9.0$ nm, $r_b = 12.0$ nm, and $r_c = 17.0$ nm, for incident photon with energy $\hbar\omega_\mathrm{l} = 0.28$ eV, where: $\left(\sigma_\mathrm{s}^-,\sigma_\mathrm{l}^-\right)$ (Fig. 3(a)), $\left(\sigma_\mathrm{s}^+,\sigma_\mathrm{l}^+\right)$ (Fig. 3(b)), $\left(\sigma_\mathrm{s}^-,\sigma_\mathrm{l}^+\right)$ (Fig. 3(c)). If we compare the contribution $\left(\sigma_\mathrm{s}^-,\sigma_\mathrm{l}^-\right)$ (Fig. 3(a)) with the contribution $\left(\sigma_\mathrm{s}^+,\sigma_\mathrm{l}^+\right)$ (Fig. 3(b)), we can see that the intensity of the resonant singularities is smaller, moreover it can also be noted that the position of singularities change. This is because the two figures correspond to two different polarizations of secondary radiation, $\sigma_\mathrm{s}^\pm$, which affects the selection rules of $m\pm1 = m'$. As we can see, the position of singularities in the graph is related to the "gap" between the two energy levels involved, while the peak intensity is mainly related to the probability of the transition and the detuning (see Ref. [29]), if the incident radiation $(\hbar\omega_\mathrm{l})$ is the same. When comparing Fig. 2(c) with Figs. 2(a) and 2(b), it is easy to see

that the intensity of the resonant singularity is higher by almost an order of magnitude, that being the reason for the main contribution to the differential cross section. Also, we can see that the resonant singularities in polarizations $\left(\sigma_s^+, \sigma_l^+\right)$ and $\left(\sigma_s^-, \sigma_l^+\right)$ are the same, this is because the secondary radiation fulfills in both cases the identical selection rule.

Moreover, figure 4 shows the emission spectrum for an electron Raman scattering process in double quantum well wire for incident photon energy $\hbar\omega_l = 0.28$ eV and polarization $\left(\sigma_s^-, \sigma_l^+\right)$. In Fig. 4(a), the dashed line corresponds to $r_a = 8.0$ nm, $r_b = 10.0$ nm, and $r_c = 15.0$ nm, while the solid line corresponds to $r_a = 9.0$ nm, $r_b = 10.0$ nm, and $r_c = 15.0$ nm. In Fig. 4(a), the dashed line corresponds to $r_a = 8.0$ nm, $r_b = 10.0$ nm, and $r_c = 16.0$ nm, while the solid line corresponds to $r_a = 8.0$ nm, $r_b = 12.0$ nm, and $r_c = 17.0$ nm. In Fig. 4(b), the dashed line has been multiplied by 10. As it can be seen in Fig. 4(a) that the increase of the radius of the wire, r_a, causes an increase in the number of singularities and position changing of singularities, which we can already see in the spectrum, and these singularities move to a lower energy position. This is because the increase of r_a increases the number of quantum states "within" the system, especially those mainly related to the wire, while the gap between different subbands decreases (see Eq. (14)). This is corroborated if we observe the resonant singularity denoted by $\hbar\omega_s(1,1,0,1)$ in both figures. In addition, in Fig. 4(b), we maintain a constant radius of the wire, $r_a = 8.0$ nm, and change the width of the shell and the barrier. However, the position of the singularity $\hbar\omega_s(1,1,0,1)$, remains constant (also, note the dashed line in Fig. 4(a); this confirms that the quantum states $m = 1, n = 1$ and $m = 1, n = 1$ belong mainly to the wire. If we look at the singularity $\hbar\omega_s(1,2,0,1)$, this moves to a position of greater energy, which is because the quantum state labeled as $m = 1$, $n = 2$, is mainly related to the shell. Furthermore, we can compare the dashed line in Fig. 4(a) with the dashed line in Fig. 4(b). In this case, the width of the shell is increased by r_c, increasing and it causes a similar effect to the one described in Fig. 4(a), but mainly affecting quantum states of the shell, allowing the occurrence of singularities related to the ones with the energy levels of the shell. Whereby, we clarify that the increase of r_a mainly affects the energy levels belonging to the wire, while the increase of r_c primarily affects the energy levels belonging to the shell. Finally, the dashed line in Fig. 4(a) and the solid line in Fig. 4(b) can be compared. We can see that the increment of the barrier, b, keeping a constant width, d, only causes a small change in the position of the resonant peak, which corresponds with that observed in Fig. 2, but affects the intensity of the singularities.

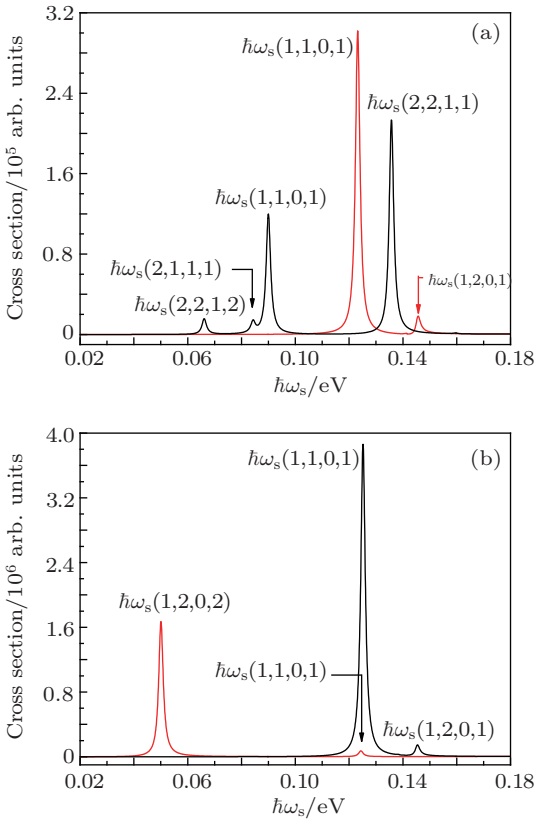


Fig. 4. (color online) The emission spectrum for an electron Raman scattering process in double quantum well wire for incident photon energy $\hbar\omega_l = 0.28$ eV and polarization $\left(\sigma_s^-, \sigma_l^+\right)$, where: (a) the dashed line corresponds to $r_a = 8.0$ nm, $r_b = 10.0$ nm, and $r_c = 15.0$ nm, while the solid line corresponds to $r_a = 9.0$ nm, $r_b = 10.0$ nm, and $r_c = 15.0$ nm; (b) the dashed line corresponds to $r_a = 8.0$ nm, $r_b = 10.0$ nm, and $r_c = 16.0$ nm, while the solid line corresponds to $r_a = 8.0$ nm, $r_b = 12.0$ nm, and $r_c = 17.0$ nm. In panel (b), the dashed line has multiplied by 10.

The change in the intensity of differential cross section for an electron Raman scattering process in semiconductor double quantum well wire is related to the coupling between the wire and the shell. This is evidently shown in Fig. 5, in which a transition rate that describes the following process is shown: first, an electron in the conduction band absorbs a photon of incident radiation, resulting in a transition from initial state $m'' = 0$, $n'' = 1$ to intermediate state $m' = 1$, $n' = 1$; then, the electron emits a photon of secondary radiation due to a new transition, from intermediate state $m' = 1$, $n' = 1$ to final state $m = 0$, $n = 2$. It is important to note that the net Raman gain in this case is directly proportional to the transition rate, this is $|T_-(0,1)\,T_+(1,0)|^2$. Then, figure 5 shows the rate transition to a wire for a double quantum well, where the barrier b varies while the fixed values of r_a and d remain. In addition, we must note that the solid line corresponds to a double quantum well where $r_a = 8.0$ nm and $d = 6.0$ nm, being the dash line the one that corresponds to a double quantum well where $r_a = 8.0$ nm and $d = 8.0$ nm. These curves are much like those obtained from an asymmetric multiple quantum well[32] and different from those obtained for a step-quantum well;[29] this is because the double quantum well wire can be decoupled

as the asymmetric multiple quantum well, but in the present case the coupling is weakened much faster. Summarizing, the coupling in a double quantum well wire with cylindrical symmetry is weaker than an asymmetrical double quantum well. In addition, it is noted that any change in the system parameters causes strong changes in the transition rate, making this system very difficult to optimize. However, although the coupling is weak in this system, the transition rate is larger than the one obtained for the asymmetrical double quantum well, observed in Fig. 6 in Ref. [32], which is due to the symmetry of the system. We should clarify that when we refer to the coupling, we are referring to the interaction between the parts of the active region of the system, which in this case are the wire and the shell. This interaction affects the electronic states of the system, so that the electronic states are a mix between wire electron states and shell electron states.

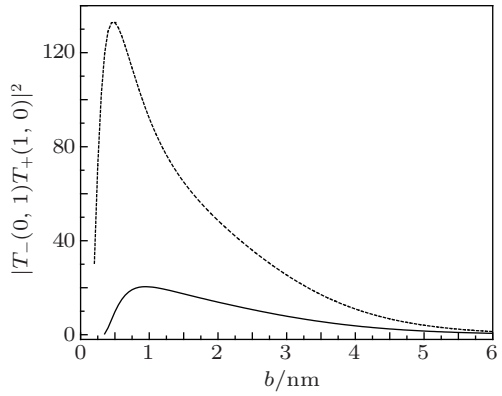


Fig. 5. The transition rate, $|T_-(0,1)T_+(1,0)|^2$, of a double quantum well wire, where the barrier $b = r_b - r_a$ varies while r_a and $d = r_c - r_b$ are fixed. The solid line corresponds to $r_a = 8.0$ nm and $d = 6.0$ nm, while the dash line corresponds to $r_a = 8.0$ nm and $d = 8.0$ nm.

5. Conclusions

In this work, we presented the formulas of calculating the electron Raman scattering intensities for the semiconductor double quantum well wire with a cylindrical cross-section, grown in a $GaAs/Al_{0.35}Ga_{0.65}As$ matrix. Moreover, we demonstrated that the structure of differential cross-section as given in figures, provides a transparent understanding of the energy subband structure. Furthermore, we showed that any change in the system configuration leads to changes in the intensity and the frequency of the secondary radiation, as well as the net Raman gain. This effectively shows that Raman spectroscopy is a powerful probe for semiconductor nanostructures due to the material-selective resonant enhancement. In addition, we can see that in this work we have applied a simplified model for the electron structure of the system. In a more realistic case, we should consider a coupled band structure by using models like the Luttinger–Kohn or the Kane model. Anyway, this band model allows us to analyze the main features of this system easily.

References

[1] Betancourt-Riera R, Riera R, Marín J L and Rosas R A 2004 *Electron Raman Scattering in Nanostructures, Encyclopedia of Nanoscience and Nanotechnology* (Stevenson Ranch: American Scientific Publishers) (Vol. 3) p. 101
[2] Kushwaha M S 2001 *Surf. Sci. Rep.* **41** 1
[3] Riera R, Marín J L and Rosas R A 2001 *Optical Properties and Impurity States in Nanostructured Materials, Handbook of Advanced Electronic and Photonic Devices* (New York: Academic) (Vol. 6) (Chapter 6)
[4] Betancourt-Riera R, Betancourt-Riera R, Nieto J J M and Riera R 2013 *Physica B* **410** 126
[5] Betancourt-Riera R, Betancourt-Riera R, Rosas R and Riera R 2012 *J. Comput. Theor. Nanosci.* **9** 1
[6] Lu F, Liu C H and Guo Z L 2012 *Physica B* **407** 165
[7] Zhai L X, Wang Y and Liu J J 2011 *J. Appl. Phys.* **110** 043701
[8] Zhong Q H and Yi X H 2010 *Superlatt. Microstruct.* **47** 723
[9] Zhong Q H, Liu C H, Zhang Y Q and Sun H C 2008 *Phys. Lett. A* **372** 2103
[10] Scheinert M, Sigg H and Tsujino S 2007 *Appl. Phys. Lett.* **91** 131108
[11] Ismailov T G and Mehdiyev B H 2006 *Physica E* **31** 72
[12] Bergues J M, Betancourt-Riera R, Riera R and Marin J L 2000 *J. Phys.: Condens. Matter* **12** 7983
[13] Bergues J M, Betancourt-Riera R, Marin J L and Riera R 1996 *Phys. Low-Dimens. Struct.* **7/8** 81
[14] Riera R, Comas F, Trallero-Giner C and Pavlov S T 1988 *Phys. Status Solid B* **148** 533
[15] Comas F, Trallero G C and Perez-Alvarez R 1986 *J. Phys. C: Solid State Phys.* **19** 6479
[16] Trallero-Giner C, Ruf T and Cardona M 1990 *Phys. Rev. B* **41** 3028
[17] González de la Cruz G and Trallero-Giner C 1998 *Phys. Rev. B* **58** 9104
[18] Wang M L, Zhang C X, Wu Z L, Jing X L and Xu H J 2014 *Chin. Phys. B* **23** 067802
[19] Jiang S M, Wu D J, Wu X W and Liu X J 2014 *Chin. Phys. B* **23** 047807
[20] Wang M, Tian Y, Zhang J M, Guo C F, Zhang X Z and Liu Q 2014 *Chin. Phys. B* **23** 087803
[21] Shi L K and Lou W K 2014 *Chin. Phys. Lett.* **31** 067304
[22] Zhong Q H and Sun Y T 2011 *Thin Solid Films* **519** 8178
[23] Wang J, Demangeot F, Pechou R, Ponchet A, Cros A and Daudin B 2012 *Phys. Rev. B* **85** 155432
[24] Livneh T, Zhang J P, Cheng G S and Moskovits M 2006 *Phys. Rev. B* **74** 035320
[25] Laneuville V, Demangeot F, Pchou R, Salles P, Ponchet A, Jacopin G, Rigutti L, de Luna Bugallo A, Tchernycheva M, Julien F H, March K, Zagonel L F and Songmuang R 2011 *Phys. Rev. B* **83** 115417
[26] Liu H L, Chen C C, Chia C, Yeh C C, Chen C H, Yu M Y, Keller S and DenBaars S P 2001 *Chem. Phys. Lett.* **345** 245
[27] Betancourt-Riera R, Betancourt-Riera R, Nieto J J M and Riera R 2015 *Chin. Phys. B* **24** 117302
[28] Betancourt-Riera R, Nieto J J M, Riera R, Betancourt-Riera R and Rosas R 2008 *J. Phys.: Condens. Matter* **20** 045203
[29] Ferrer-Moreno L A, Betancourt-Riera R, Betancourt-Riera R and Riera R 2015 *Physica B* **477** 87
[30] Abramowitz M and Stegun I A 1972 *Handbook of Mathematical Functions with Formulas, Graphs, and Mathematical Tables* (New York: Dover Publications)
[31] Bergues J M, Riera R, Comas F and Trallero-Giner C 1995 *J. Phys.: Condens. Matter* **7** 7273
[32] Betancourt-Riera R, Rosas R, Marín-Enriquez I, Riera R and Marin J L 2005 *J. Phys.: Condens. Matter* **17** 4451
[33] Betancourt-Riera R, Riera R, Rosas R and Nieto J M 2008 *Physica E* **40** 785